Available online at www.sciencedirect.com
SCIENCE DIRECT®
ELSEVIER
International Journal of Solids and Structures 41 (2004) 6407–6427
INTERNATIONAL JOURNAL OF SOLIDS and STRUCTURES
www.elsevier.com/locate/ijsolstr

Buckling of stiffened plates with bulb flat flanges

D.A. Danielson *, A. Wilmer

Department of Applied Mathematics, Naval Postgraduate School, Monterey, CA 93943, USA

Received 22 September 2003; received in revised form 25 May 2004
Available online 2 July 2004

Abstract

The subject of this research is the buckling behavior of a rectangular plate, with a bulb flat stiffener attached to one side of the plate. The stiffener cross section has a thin web and a bulb flat flange that extends to one side of the web. The stiffened plate structure is subjected to axial compression that increases to the buckling load. Results of the investigation include planar property formulas for the asymmetric flange geometry, an analytic expression for the Saint-Venant torsional constant of the flange cross section, and an analytic expression for the buckling stress corresponding to a tripping mode of the structure. The torsional constant for the bulb flat stiffener is 15–23% higher than understood previously. The analytic expression for the buckling stress of a bulb flat stiffened plate differs by less than 4% from finite element and experimental results.
Published by Elsevier Ltd.

Keywords: Ship structures; Grillages; Stiffened plates; Buckling; Bulb flat; Saint-Venant; Torsion; Steel; Elasticity

1. Introduction

Stiffened plates are basic structural components of many items, including bridges, buildings, automobiles, aircraft, offshore platforms, and naval vessels. In ship design, a stiffener is a metal structure composed of a web and flange. Stiffeners placed on one or both sides of a plate add strength and hinder overall collapse of the plate panel. Because of the structural complexity of stiffened plates, understanding their elastic instability is of great importance to ship designers.

Stiffened plate investigations occur in three general forms: theoretical, using classical and emerging theory; numerical, using finite element methods and computer-aided simulation; and experimental, using actual grillages. With regard to bulb flat stiffened plates, it appears that most of what is known of their behavior comes from numerical and experimental investigations. This investigation attempts to contribute new theoretical insights into the behavior of bulb flat stiffened plates.

The use of bulb flat plate stiffeners in ship design is said to reduce building time and maintenance cost. Companies that produce bulb flat plate stiffeners manufacture each stiffener as a single unit, which

* Corresponding author. Tel.: +1-831-6562622; fax: +1-831-6562355.
E-mail address: dad@nps.edu (D.A. Danielson).

0020-7683/$ - see front matter. Published by Elsevier Ltd.
doi:10.1016/j.ijsolstr.2004.05.063

reportedly results in less production cost compared to welded or fabricated stiffeners. Additionally, the curved surface of the bulb flat stiffener traps less moisture resulting in less corrosion. The shape of the bulb flat stiffener is much easier to inspect, weld, and paint. These benefits save significant repair and maintenance costs over the lifetime of the vessel.

A complete review of the literature on buckling of stiffened plates has been given in a series of papers by Danielson et al. (1990, 1993, 1994) and Danielson (1995), analyzing the tripping of stiffened plates. Our previous work also included finite element investigations of the buckling loads and modes of ship grillages with various dimensions (Danielson and Kihl, 1996, 1997).

The only published work on the topic of the buckling behavior of bulb flat plates is apparently that of Chou (1997), Chou and Chapman (2000) and Chou et al. (2000). They state that the British Standards Institute design criteria for bulb flat stiffeners are unduly conservative. Their study presents an iterative method for obtaining the critical modes and stresses. They validate the study using FINASIC, a finite element program, and compare the results to actual tests on cruciform struts and box columns containing bulb flat stiffeners.

An interesting aspect of their theoretical analysis is the idealization of the bulb flat flange as an equivalent angle flange. That is, they treat the bulb flat cross section like a rectangular cross section in regards to the bulb flat torsional and warping properties. We address this treatment and show that idealization imputes error in the calculation of the bulb flat cross section's torsional rigidity. Developing and using expressions that maintain the bulb flat geometry yields more accurate cross sectional property data resulting in a more accurate analysis.

In the current paper, we extend our earlier work to apply to plates having stiffeners with bulb flat flanges. Our previous investigations were based on the assumption that the stiffener cross section does not deform in its plane. Applying nonlinear beam theory to the stiffeners, we obtained analytic expressions for the tripping stresses of stiffened plate structures. We now model the stiffener webs with plate theory and the stiffener flanges with beam theory. Since the stiffener cross section is allowed to deform, we obtain lower buckling stresses than would be obtained by modeling the entire stiffener with beam theory.

2. Bulb flat flange cross sectional boundary and planar properties

Consider the cross section of a bulb flat that extends to one side of the web as shown in Figs. 1 and 2. Fig. 1 shows only the flange horizontally oriented. Fig. 2 shows the entire stiffener cross section composed

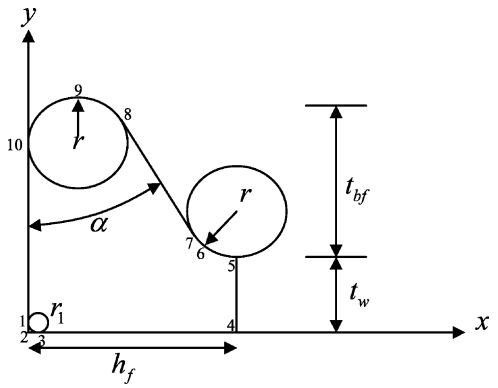

Fig. 1. Bulb flat flange geometry.

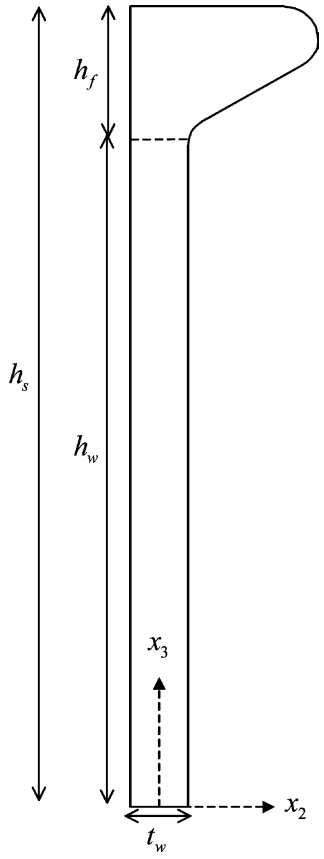

Fig. 2. Bulb flat stiffener cross section.

of the bulb flat flange and thin web. Five independent variables (t_w, t_{bf}, r, r_1, and α) uniquely determine the flange boundary. The variable t_w denotes the web thickness defined by the vertical distance between point 4 and point 5. The variable t_{bf} denotes the bulb thickness defined by the vertical distance between point 9 and a point horizontal to point 5. The total flange thickness (at its maximum value) is denoted by $t_f = t_w + t_{bf}$ defined by the vertical distance between point 9 and the line formed by points 3 and 4. The corners of the cross section have radii of curvature r and r_1. Points 5–6–7 and 8–9–10 define the corners with radius of curvature r. Points 1–2–3 define the corner with radius r_1. The cross section has a flat portion defined by the points 7 and 8, that slopes α degrees from the y-axis.

Let h_f denote the flange height. The boundary of the flange includes two vertical sides $x = 0$ and $x = h_f$, where $h_f = t_{bf}\tan\alpha + r(1 - 2\tan\alpha + 2\sec\alpha)$ and $0 < \alpha < \pi/2$ (see Appendix A of Wilmer, 2003). The upper boundary of the flange cross section is given by

$$f(x) = \begin{cases} f_1(x) = (t_w + t_{bf} - r) + \sqrt{r^2 - (x-r)^2}, & 0 \leqslant x < r + r\cos\alpha \\ f_2(x) = -x\cot\alpha + t_w + t_{bf} + r(\cot\alpha + \csc\alpha - 1), & r + r\cos\alpha \leqslant x < h_f - r\cos\alpha \\ f_3(x) = (t_w + r) - \sqrt{r^2 - (x - h_f)^2}, & h_f - r\cos\alpha \leqslant x \leqslant h_f \end{cases} \quad (1)$$

The lower boundary of the flange cross section is given by

$$g(x) = \begin{cases} g_1(x) = r_1 - \sqrt{r_1^2 - (x - r_1)^2}, & 0 \leqslant x < r_1 \\ g_2(x) = 0, & r_1 \leqslant x \leqslant h_f \end{cases} \tag{2}$$

Appendix B of Wilmer (2003) and Appendix B of Kihl (2003) contain a summary of the general planar property formulas. For brevity, the general formulas are omitted here. The formulas can be specialized for a class of bulb flat flange cross sections by assigning a value to one or more of the variables. For example, setting $\alpha = \pi/6$ defines planar property formulas for a class of bulb flat cross sections with a 30° slope. Additionally, if the radius of curvature of the cross section corner r_1 is assumed to be one-tenth of the web thickness t_w ($r_1 = t_w/10$), terms involving r_1 become negligible. The following formulas are algebraic expansions for this specialized class of bulb flat flanges. The flange area and centroid formulas are

$$A_f = -\left(1 - \frac{\pi}{4}\right)r^2 + \left[\left(1 + \frac{2\sqrt{3}}{3}\right)t_w + \left(1 + \frac{\sqrt{3}}{3}\right)t_{bf}\right]r + \frac{\sqrt{3}}{6}t_{bf}^2 + \frac{\sqrt{3}}{3}t_w t_{bf}$$

$$\bar{x} = \left[\left(\frac{\pi}{4} - \frac{\pi\sqrt{3}}{9} - \frac{2}{9}\right)r^3 + \left(\frac{7}{6} + \frac{2\sqrt{3}}{3}\right)r^2 t_w + \left(1 + \frac{\sqrt{3}}{3} - \frac{\pi\sqrt{3}}{18}\right)r^2 t_{bf} + \left(\frac{2 + \sqrt{3}}{3}\right)r t_w t_{bf} + \left(\frac{1 + \sqrt{3}}{6}\right)r t_{bf}^2 + \frac{1}{6}t_w t_{bf}^2 + \frac{1}{18}t_{bf}^3\right]\frac{1}{A_f}$$

$$\bar{y} = \left[\left(\frac{11\sqrt{3}}{18} - \frac{7\pi}{12} + \frac{5}{6}\right)r^3 + \left(\frac{\pi}{4} - 1\right)r^2 t_w + \left(\frac{5\pi}{12} - 1 - \frac{\sqrt{3}}{3}\right)r^2 t_{bf} + \left(\frac{1}{2} + \frac{\sqrt{3}}{3}\right)r t_w^2 + \left(1 + \frac{\sqrt{3}}{3}\right)r t_w t_{bf} + \left(\frac{1}{2} + \frac{\sqrt{3}}{6}\right)r t_{bf}^2 + \frac{\sqrt{3}}{6}t_w^2 t_{bf} + \frac{\sqrt{3}}{6}t_w t_{bf}^2 + \frac{\sqrt{3}}{18}t_{bf}^3\right]\frac{1}{A_f}$$

Formulas for the moments of inertia about the axes and centroid for the specialized class of flanges are

$$I_x = \left(-1 + \frac{5\pi}{16}\right)r^4 + \left[\left(\frac{5}{3} + \frac{11\sqrt{3}}{9} - \frac{7\pi}{6}\right)t_w + \left(\frac{11\sqrt{3}}{18} + \frac{5}{3} - \frac{5\pi}{6}\right)t_{bf}\right]r^3 + \left[\left(-1 + \frac{\pi}{4}\right)t_w^2 + \left(-\frac{2\sqrt{3}}{3} - 2 + \frac{5\pi}{6}\right)t_w t_{bf} + \left(-1 + \frac{5\pi}{12} - \frac{\sqrt{3}}{3}\right)t_{bf}^2\right]r^2 + \left[\left(\frac{2\sqrt{3}}{9} + \frac{1}{3}\right)t_w^3 + \left(\frac{\sqrt{3}}{3} + 1\right)\left(t_w^2 t_{bf} + t_w t_{bf}^2\right) + \left(\frac{\sqrt{3}}{9} + \frac{1}{3}\right)t_{bf}^3\right]r + \frac{\sqrt{3}}{36}t_{bf}^4 + \frac{\sqrt{3}}{6}t_w^2 t_{bf}^2 + \frac{\sqrt{3}}{9}t_w t_{bf}^3 + \frac{\sqrt{3}}{9}t_w^3 t_{bf}$$

$$I_y = \left(\frac{11\sqrt{3}}{27} - \frac{2\pi\sqrt{3}}{9} + \frac{2}{9} + \frac{13\pi}{144}\right)r^4 + \left[\left(\frac{26\sqrt{3}}{27} + \frac{5}{3}\right)t_w + \left(\frac{43\sqrt{3}}{54} + \frac{4}{3} - \frac{2 + \sqrt{3}}{9}\pi\right)t_{bf}\right]r^3 + \left[\left(\frac{7\sqrt{3}}{9} + \frac{4}{3}\right)t_w t_{bf} + \left(\frac{1 + \sqrt{3}}{3} - \frac{\pi}{18}\right)t_{bf}^2\right]r^2 + \left[\left(\frac{2\sqrt{3}}{9} + \frac{1}{3}\right)t_w t_{bf}^2 + \left(\frac{\sqrt{3}}{27} + \frac{1}{9}\right)t_{bf}^3\right]r + \frac{\sqrt{3}}{27}t_w t_{bf}^3 + \frac{\sqrt{3}}{108}t_{bf}^4$$

$$I_c = I_x + I_y - A_f(\bar{x}^2 + \bar{y}^2)$$

3. Bulb flat flange torsion properties

The Saint-Venant torsional constant J can be obtained relatively easily for flanges with cross sections that are symmetric about at least one axis. For instance, for rectangular cross sections with length $2b$ and thickness $2a$, the exact torsional constant is (Timoshenko and Goodier, 1970)

$$J = \frac{1}{3}(2b)(2a)^3\left(1 - \frac{192a}{\pi^5 b}\sum_{n=1,3,5,\ldots}^{\infty}\frac{1}{n^5}\tanh\frac{n\pi b}{2a}\right) \tag{3}$$

For flanges with arbitrary cross sections, finding the exact solution to the torsion problem is quite difficult. The reason for this is, as Donaldson (1993) notes: "It is not difficult to write expressions that satisfy the governing differential equation, and it is not difficult to write expressions that satisfy the boundary conditions. What is difficult is to do both simultaneously."

Saint-Venant [1] offers an approximate expression for the torsional constant of any solid section (except certain common sections):

$$J \approx \frac{1}{4\pi^2}\frac{A^4}{I_c}$$

When applied to bulb flat flange cross sections, this Saint-Venant approximation generates torsion values that differ significantly from values obtained by finite element methods. However, this expression led us to a similar formula with a multiplicative constant different from $1/4\pi^2 \approx 0.0253$.

Corus Group [2] provides a special profile brochure (2002) that contains technical data on 59 bulb flat cross sections, with flanges having geometry within the aforementioned class. The following analytical formula well approximates the finite element results for the torsional constant of all 59 bulb flat flanges, and is used throughout the remainder of this investigation:

$$J_f \approx 0.0231\frac{A_f^4}{I_c} \tag{4}$$

4. Validation of the property formulas using finite element models

Analysis of several finite element models using MSC Nastran 2001/Patran 2001-r3 software serves to validate the property formulas. The property values from formulas are compared to values from finite element models. In each finite element bulb flat flange model, 10 distinct points establish the boundary of the bulb flat flange cross section. Straight lines and three-point arc curves are defined from the boundary points. A single trimmed surface is defined from the curves. The arbitrary shape option in the software's beam library is used with the maximum allowable curvature error set at 0.005. Maple 8 computer environment and a handheld calculator are used to calculate formula results.

Fig. 3 shows the bulb flat flange, while Fig. 4 shows the flange and web together. The area A_f of each *angle* flange is chosen to be identical to its corresponding bulb flat flange, and the height h_s of each *angle* stiffener is chosen to be identical to its corresponding bulb flat stiffener.

[1] Discussed by Saint-Venant, "Sur une formule donnant approximativement le moment de torsion", *Comptes Rendus*, vol. 88, 1879, pp. 142–154, and in Timoshenko and Goodier (1970).

[2] Corus Group was formed in 1999 through the merger of British Steel and Koninklijke Hoogovens. The company is a leading international metal company and one of the world's leading producers of bulb flat profiled metals.

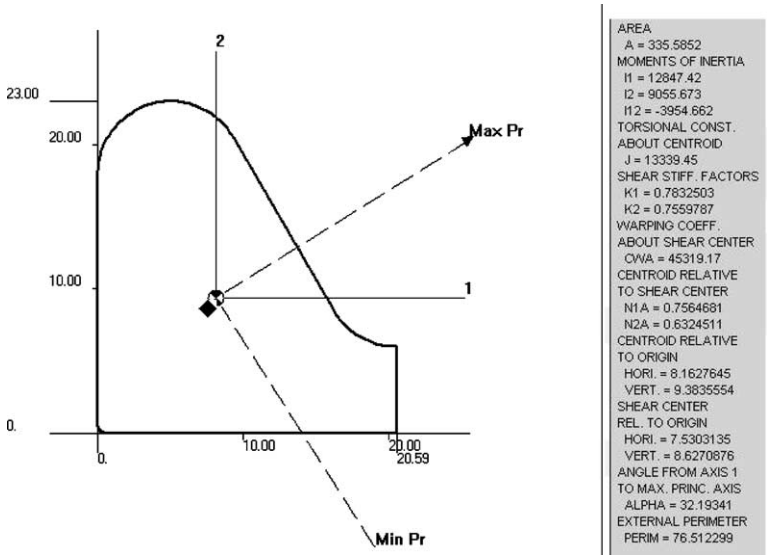

Fig. 3. MSC Patran graph and data of a horizontal bulb flat flange.

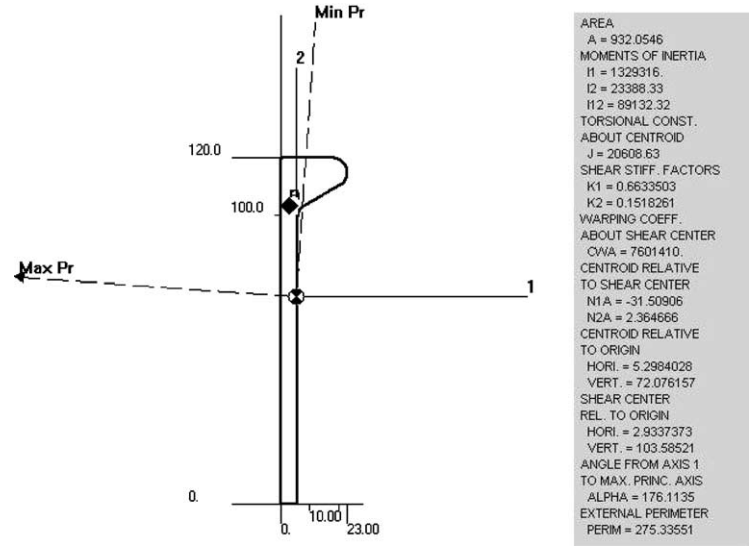

Fig. 4. MSC Patran graph and data of a bulb flat stiffener model.

Table 1 presents planar property values for several bulb flat flanges using expression (4) and formulas in Wilmer (2003). The table presents a comparison of the formula values to data obtained from MSC Nastran/Patran finite element models of the cross sections. Examination of Table 1 reveals several noteworthy aspects. The formula results agree with the finite element results for the bulb flat flange. The two independent sources agree almost exactly on the centroid locations $(\overline{x}, \overline{y})$, the flange area values A_f, and the values for the polar moments I_c. Though not independent, the formula values for the torsional constants J_f obtained using the approximate expression (4) differ from the finite element values by less than 1/2%. Such agreement supports the validation of the formula expressions.

Table 1
Comparison of flange values

Source	t_w (mm)	t_{bf} (mm)	r (mm)	$\bar{x}$ (mm)	$\bar{y}$ (mm)	A_f (mm^2)	I_c (mm^4)	Percent change	J_f (mm^4)	Percent change
Formula	6.0	17.0	5.0	8.163	9.384	335.59	21,904	*	13,376	0.28%
FE (bulb)				8.163	9.384	335.59	21,903	*	13,339	*
FE (angle)				7.730	10.267	335.59	24,199	10.48%	13,973	4.75%
Formula	8.0	17.0	5.0	8.397	10.251	376.71	27,481	*	16,928	0.08%
FE (bulb)				8.397	10.251	376.70	27,480	*	16,915	*
FE (angle)				8.010	11.035	376.71	30,560	11.21%	16,026	−5.26%
Formula	7.0	19.0	5.5	9.081	10.608	422.19	34,722	*	21,137	0.29%
FE (bulb)				9.081	10.607	422.19	34,720	*	21,076	*
FE (angle)				8.611	11.581	422.19	38,450	10.74%	21,586	2.42%
Formula	10.0	19.0	5.5	9.408	11.922	490.54	46,670	*	28,661	−0.19%
FE (bulb)				9.408	11.921	490.54	46,667	*	28,716	*
FE (angle)				9.000	12.754	490.54	52,004	11.44%	26,362	−8.20%
Formula	7.0	22.0	6.0	10.036	11.789	519.51	53,122	*	31,674	0.29%
FE (bulb)				10.036	11.789	519.50	53,120	*	31,583	*
FE (angle)				9.486	12.992	519.51	58,776	10.65%	33,449	5.91%
Formula	9.0	22.0	6.0	10.287	12.642	570.70	63,914	*	38,339	0.20%
FE (bulb)				10.287	12.642	570.69	63,911	*	38,262	*
FE (angle)				9.784	13.735	570.70	71,244	11.47%	36,965	−3.39%
Formula	8.0	25.0	7.0	11.574	13.429	681.94	91,186	*	54,785	0.26%
FE (bulb)				11.574	13.428	681.93	91,182	*	54,641	*
FE (angle)				10.939	14.786	681.94	100,732	10.47%	58,328	6.75%
Formula	10.0	25.0	7.0	11.829	14.281	740.89	107,321	*	64,856	0.25%
FE (bulb)				11.829	14.281	740.89	107,316	*	64,696	*
FE (angle)				11.243	15.528	740.90	119,359	11.22%	63,541	−1.79%

Variables t_w, t_{bf}, and r are given. $r_1 = (1/10)t_w$ and $\alpha = \pi/6$ rad. Percent change in $J_f = \frac{J_f - J_f^{(FE)}}{J_f^{(FE)}} \times 100$.
* Indicates absolute percent change of less than 0.01%.

On the other hand, note that the finite element results for the bulb flat flange differ noticeably from the finite element results for an area-equivalent angle flange. The centroid coordinates $(\bar{x}, \bar{y})$ differ considerably. The moments I_c differ by 10–12%. Only the flange area results agree which is by design. This strengthens the case that using an angle flange as an area-equivalent to the bulb flat flange produces error.

To determine the values for the area and torsional constant for the stiffener that includes the web and bulb flat flange together, let the web have height h_w where $h_w = h_s - h_f$ (see Fig. 2). The stiffener area formula is given by

$$A_s = A_f + A_w = A_f + h_w t_w$$

The membrane analogy for uniform torsion is a useful tool for visualizing the distribution of shearing stress in beam cross sections and provides justification for approximating the torsional constant of the stiffener. If a membrane of constant thickness were stretched over a beam cross section, fixed against the boundary of the cross section, and filled with a gas exerting normal pressure on the membrane surface, the volume under the membrane would be proportional to the torque-carrying capacity of the cross section. It follows from the membrane analogy that the torque-carrying capacity of a cross section composed of several components is greater, but not much greater, than the sum of the components treated separately.

Hence, the total torsional constant of the entire stiffener is approximated by the sum of the first term in (3) and the empirical formula (4):

$$J_s \approx J_w + J_f = \frac{1}{3} h_w t_w^3 + 0.0231 \frac{A_f^4}{I_c} \tag{5}$$

Table 2 compares the area and torsional constant calculations with finite element model results. Also, Table 2 compares the area and torsional constant calculations to published data from the Corus technical brochure (2002). Each stiffener model contains four rows of results, referred to as a result set for clarity. Each row is data from a different source. The first row in each result set is data from the formulas for the bulb flat cross section. The second row in each set is data from the finite element

Table 2
Comparison of stiffener values

Source	t_w (mm)	t_{bf} (mm)	r (mm)	h_s (mm)	A_s (mm^2)	$I_{c\text{-stifffener}}$ (mm^4)	Percent change	J_s (mm^4)	Percent change
Formula	6.0	17.0	5.0	120.0	932.06	1,352,719	*	20,534	−0.37%
FE (bulb)					932.05	1,352,704	*	20,609	*
FE (angle)					932.06	1,369,171	1.27%	18,043	−12.45%
Corus					931.00	1,353,400	0.05%	15,950	−22.61%
Formula	8.0	17.0	5.0	120.0	1172.00	1,676,051	*	33,894	−0.91%
FE (bulb)					1172.00	1,676,034	*	34,204	*
FE (angle)					1172.00	1,694,072	1.08%	30,413	−11.08%
Corus					1170.00	1,681,000	0.30%	27,730	−18.93%
Formula	7.0	19.0	5.5	140.0	1242.45	2,448,920	*	34,535	−0.46%
FE (bulb)					1242.44	2,448,895	*	34,694	*
FE (angle)					1242.44	2,475,783	1.10%	30,482	−12.14%
Corus					1240.00	2,448,000	−0.04%	27,080	−21.95%
Formula	10.0	19.0	5.5	140.0	1662.34	3,206,519	*	67,721	−1.25%
FE (bulb)					1662.33	3,206,493	*	68,575	*
FE (angle)					1662.34	3,236,434	0.93%	61,791	−9.89%
Corus					1660.00	3,215,600	0.28%	57,520	−16.12%
Formula	7.0	22.0	6.0	160.0	1460.10	3,788,414	*	47,037	−0.26%
FE (bulb)					1460.09	3,788,380	*	47,160	*
FE (angle)					1460.10	3,831,830	1.15%	41,325	−12.37%
Corus					1460.00	3,788,600	*	36,810	−21.95%
Formula	9.0	22.0	6.0	160.0	1780.03	4,558,106	*	70,991	−0.65%
FE (bulb)					1780.02	4,558,068	*	71,453	*
FE (angle)					1780.03	4,605,079	1.03%	63,240	−11.49%
Corus					1780.00	4,553,200	−0.11%	57,630	−19.35%
Formula	8.0	25.0	7.0	180.0	1885.81	6,188,305	*	70,468	−0.26%
FE (bulb)					1885.80	6,188,242	*	80,674	*
FE (angle)					1885.81	6,261,495	1.18%	70,710	−12.35%
Corus					1890.00	6,189,000	0.01%	63,520	−21.26%
Formula	10.0	25.0	7.0	180.0	2245.73	7,289,798	*	115,017	−0.57%
FE (bulb)					2245.72	7,289,731	*	115,672	*
FE (angle)					2245.73	7,368,371	1.08%	102,123	−11.71%
Corus					2250.00	7,290,500	0.01%	93,280	−19.36%

Variables t_w, t_{bf}, r, and h_s are given. $r_1 = (1/10)t_w$ and $\alpha = \pi/6$ rad. Percent change in $J_s = \frac{J_s - J_s^{(FE)}}{J_s^{(FE)}} \times 100$.
* Indicates absolute percent change of less than 0.01%.

analysis for the bulb flat cross section. The third row in each set is data from the finite element analysis for the area-equivalent angle cross section. The fourth row in each set is data from the Corus technical data brochure.

Comparing the first two rows of each stiffener result set compares the formula results to the finite element results. The independent sources agree almost exactly on the stiffener area values A_s and the values for the polar moments $I_{\text{c-stiffener}}$. The formula values for the torsional constants $J_{\text{stiffener}}$ obtained using the approximate expression (5) differ from the finite element values by less than 2%.

Comparing the second and third rows of each stiffener result set compares the finite element results of the bulb flat stiffener to the finite element results of the area-equivalent angle stiffener. The two sources agree on the stiffener area values and the values for the polar moments. However there is a marked difference in the torsional constant values. Comparing the second and fourth rows of each stiffener result set compares the finite element results of the bulb flat to the Corus technical data. The sources agree on the stiffener area values A_s and the values for the polar moments. However, the Corus data underestimates the torsional constant values by 16–23%. The reason for the discrepancy appears to be the lack of accuracy when idealizing the bulb flat as an area-equivalent angle stiffener.

5. Derivation of the buckling equations

The energy method for the solution of elastic stability problems is based on an extremum principle of mechanics that uses an energy criterion to characterize the equilibrium condition of the elastic system. A more precise statement of the energy criterion is made in Danielson (1974) and is recapitulated in the following discussion.

Let P_{I} denote the potential energy of a system in equilibrium state I. Let P_{II} denote the potential energy in a neighborhood of equilibrium state I. Let $P[u]$ represent the increment in potential energy of the elastic system in transition by displacement field u from state I to a neighboring state. In addition, let $P[u]$ be expandable into the following component terms (functionals)

$$P_{\text{II}} - P_{\text{I}} = P[u] = P_1[u] + P_2[u] + P_3[u] + \cdots$$

where $P_1[u]$ refers to linear terms (functionals) with respect to u, $P_2[u]$ refers to quadratic terms (functionals) with respect to u, and so forth. If $P[u] > 0$ for all nonvanishing neighborhoods of displacement fields u, then the fundamental equilibrium state I is stable. In a practical sense, stability here means that a force, shock, or disturbance of the system does not cause an excessive change or dramatic departure of the equilibrium state to a neighboring state or configuration. If there exists a displacement field for which $P[u] < 0$, the fundamental equilibrium state I is unstable. Because the elastic system is in equilibrium, the linear term of the potential energy increment must vanish. That is, equilibrium requires $P_1[u] = 0$. The condition necessary for stability is $P_2[u] > 0$. The critical case of neutral equilibrium occurs when there exists a displacement field u_1 such that $P_2[u_1] = 0$ and $P_2[u \neq u_1] > 0$. In this case, the displacement field u_1 is the buckling mode, and the value of the load that corresponds to this displacement field is called the bifurcation-buckling load. Stated mathematically,

$$P_2[u] \geqslant 0 \tag{6}$$

is the criterion used to determine the buckling mode and load given the properly defined total potential energy functional for the stiffened plate structure.

Now consider a plate which is initially rectangular in shape and has several parallel stiffeners spaced a distance b apart. The structure is subjected to a uniform compressive stress σ (force per unit area of one side). We suppose that at low values of σ, the plate and stiffeners simply compress symmetrically. Our object is to find the critical stress σ_{cr} at which the stiffened plate may buckle into an alternate mode.

Our analysis is based on the following assumptions, modified from Danielson (1995):

(i) Each plate–stiffener unit of width b undergoes an identical deformation.
(ii) The plate and web obey the nonlinear Von Karman plate equations (see Timoshenko and Gere, 1961). The flange obeys the nonlinear beam equations derived by Bleich (1952). Note that these equations account for the nonlinear coupling between the axial load and bending curvature.
(iii) The plate and stiffener material is linear elastic, homogeneous, and isotropic.
(iv) Every particle on the bottom surface of a web undergoes the same displacement as the corresponding particle on the top surface of the plate, and every line of particles in a web normal to the plate surface remains normal to the deformed plate at its surface. In other words, the bases of the stiffeners are clamped to the plate.
(v) The incremental buckling extensional strains at the midsurface of the plate and web are negligible.
(vi) The incremental buckling displacements may be approximated by the fundamental harmonic in their Fourier expansions. Accuracy may be improved by including additional terms in the Fourier series, but at the expense of having to use a numerical method (see Byklum and Amdahl, 2002).
(vii) The plate and web are so thin that their thicknesses are negligible compared to their width, length, and wavelength of deformation. Hence, the plate and web can be treated as plates.
(viii) The stiffener flange has a solid cross section with a length that is much greater than its largest cross sectional dimension. Hence, the stiffener flange can be treated as a beam.
(ix) The flange undergoes only lateral bending and torsion. The entire stiffener is too stiff to undergo bending in the vertical direction.
(x) The ends of the plate and stiffener are simply supported.

Thus we study a simply supported rectangular plate of length a, width b, and thickness t_p, with a longitudinal stiffener whose ends are also simply supported. The stiffener divides the width of the plate in halves and is composed of a thin web (treated as a plate element) of height h_w and thickness t_w, and a bulb flat flange (treated as a beam-column element). For the stiffened plate structure, the Cartesian coordinate system (x_1, x_2, x_3) is adopted from our previous work to aid result comparison and to minimize confusion with the flange cross sectional coordinate systems (x, y) and (x_c, y_c). Here x_1 is distance along the plate–stiffener intersection, x_2 is measured on the plate surface, and x_3 is distance normal to the plate surface. The quadratic terms of the total potential energy functional for this single stiffened plate unit at the instance of buckling can be expressed as

$$P_2[W, V] = U_{\text{plate}} + U_{\text{web}} + U_{\text{flange}} - T_{\text{plate}} - T_{\text{web}} - T_{\text{flange}} \tag{7}$$

Here $W = W(x_1, x_2)$ and $V = V(x_1, x_3)$ are the incremental deflection fields (buckling modes) of the plate and stiffener in the x_3 and x_2 directions, respectively. Subscripts on W and V denote partial differentiation with respect to the coordinate system, e.g. $W_{12} = \frac{\partial^2 W}{\partial x_1 \partial x_2}$. In expression (7), U_i denotes the internal potential energy as a result of strains for element i, and T_i denotes the potential energy of the external loads applied to element i.

The internal potential energy expressions due to strains for the plate and web are

$$U_{\text{plate}} = \frac{1}{2} D_p \int_{-\frac{b}{2}}^{\frac{b}{2}} \int_0^a \{(W_{11} + W_{22})^2 - 2(1-\nu)[W_{11}W_{22} - W_{12}^2]\}\, dx_1\, dx_2$$

$$U_{\text{web}} = \frac{1}{2} D_w \int_0^{h_w} \int_0^a \{(V_{11} + V_{33})^2 - 2(1-\nu)[V_{11}V_{33} - V_{13}^2]\}\, dx_1\, dx_3$$

Here $D_p = Et_p^3/12(1-\nu^2)$ and $D_w = Et_w^3/12(1-\nu^2)$. The potential energy expression for the external loads applied to the plate and web are

$$T_{\text{plate}} = \frac{1}{2}\sigma t_{\text{p}} \int_{-\frac{b}{2}}^{\frac{b}{2}} \int_0^a W_1^2 \, \mathrm{d}x_1 \, \mathrm{d}x_2, \qquad T_{\text{web}} = \frac{1}{2}\sigma t_{\text{w}} \int_0^{h_{\text{w}}} \int_0^a V_1^2 \, \mathrm{d}x_1 \, \mathrm{d}x_3$$

The internal potential energy expression for the flange is

$$U_{\text{flange}} = \frac{1}{2} \int_0^a (EI_{x_{\text{c}}} V_{11}^2 + GJ_{\text{f}} V_{13}^2)_{x_3 = h_{\text{w}}} \, \mathrm{d}x_1$$

Here $G = E/2(1+v)$ and $I_{x_{\text{c}}}$ is the moment about the x_{c}-axis through the centroid:

$$I_{x_{\text{c}}} = I_x - A_{\text{f}} \overline{y}^2$$

The potential energy of the external load for the flange is derived here and follows the outline in Bleich (1952) and Chajes (1974). The potential energy of the external load for the flange is the sum of the products of the external forces and the displacements of their points of application in the direction of the forces. As the flange buckles, the stress on the end surfaces may change to $\sigma + \mathrm{d}\sigma$. Considering small deformations, the work done by $\mathrm{d}\sigma$ may be neglected in comparison with the work done by σ. The change in potential energy for each fiber in the cross section of the flange is $\mathrm{d}T_{\text{flange}} = (\sigma \, \mathrm{d}A)\delta_{\text{c}}$.

Here δ_{c} is the relative fiber displacement due to the curvature of the flange as it buckles under compression. The distance δ_{c} is equal to the difference between the arc length S of the fiber due to bending and the chord length a of the fiber ($\delta_{\text{c}} = S - a$). The potential energy of the external load for the entire flange is obtained by integrating over the cross sectional area of the flange. Thus

$$T_{\text{flange}} = \sigma \int \int_A \delta_{\text{c}} \, \mathrm{d}x_2 \, \mathrm{d}x_3.$$

To determine δ_{c}, consider a cross section of the flange at distance x_1 along the length of the flange (Fig. 5). The centroid of the cross section coincides with the $(x_{\text{c}}, y_{\text{c}})$ coordinate origin. Due to buckling, the point with coordinates $(x_{\text{c}}, y_{\text{c}})$ in the cross section of the flange will change coordinates to $(x_{\text{c}} + \Delta x_{\text{c}}, y_{\text{c}} + \Delta y_{\text{c}})$, where Δx_{c} and Δy_{c} are functions of x_1. Let the point of rotation of the cross section have coordinates (ξ, ζ) relative to the centroid of the cross section. Movements of the point of rotation define the displacement of points in the cross section: $w(x_1)$ in the x_{c}-direction, $v(x_1)$ in the y_{c}-direction, and $\beta(x_1)$ counterclockwise rotation about the point of rotation. Hence

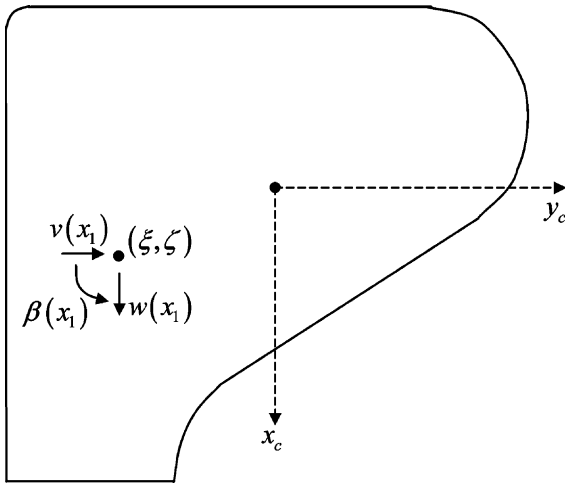

Fig. 5. Flange cross section with centroidal coordinate system.

$$\begin{bmatrix}\Delta x_c\\ \Delta y_c\end{bmatrix} = \begin{bmatrix}\cos\beta & -\sin\beta\\ \sin\beta & \cos\beta\end{bmatrix}\begin{bmatrix}x_c-\xi+w\\ y_c-\zeta+v\end{bmatrix} - \begin{bmatrix}x_c-\xi\\ y_c-\zeta\end{bmatrix}$$

Since only small deformations are considered, simplification of the right-hand side gives

$$\begin{bmatrix}\Delta x_c\\ \Delta y_c\end{bmatrix} = \begin{bmatrix}1 & -\beta\\ \beta & 1\end{bmatrix}\begin{bmatrix}x_c-\xi+w\\ y_c-\zeta+v\end{bmatrix} - \begin{bmatrix}x_c-\xi\\ y_c-\zeta\end{bmatrix} = \begin{bmatrix}w-(y_c-\zeta)\beta-v\beta\\ v+(x_c-\xi)\beta+w\beta\end{bmatrix}$$

Using the Pythagorean theorem, and considering $\frac{d\Delta x_c}{dx_1} = \Delta x_c'$ and $\frac{d\Delta y_c}{dx_1} = \Delta y_c'$ to be small, yields

$$\delta_c = S - a = \int_0^a \{[1+(\Delta x_c')^2+(\Delta y_c')^2]^{1/2} - 1\}\,dx_1 \approx \frac{1}{2}\int_0^a [(\Delta x_c')^2+(\Delta y_c')^2]\,dx_1$$

The potential energy of the external load for the flange is thus given by

$$T_{\text{flange}} = \frac{1}{2}\sigma\int\int_A\int_0^a [(\Delta x_c')^2+(\Delta y_c')^2]\,dx_1\,dx_c\,dy_c$$

Using the geometrical relations for the area, first, and second moments of the flange cross section

$$\int\int_R dx_c\,dy_c = A_f$$
$$\int\int_R x_c\,dx_c\,dy_c = \int\int_R y_c\,dx_c\,dy_c = 0$$
$$\int\int_R (x_c-\xi)^2+(y_c-\zeta)^2\,dx_c\,dy_c = I_f$$

we find that the quadratic terms of the potential energy due to external loads are given by

$$T_{\text{flange}} = \frac{1}{2}\sigma\int_0^a [A_f(v'^2+w'^2) - 2A_f\xi v'\beta' + 2A_f\zeta w'\beta' + I_f\beta'^2]\,dx_1$$

Movements in the x_c-direction affected by $w(x_1)$ are assumed negligible by assumption (ix), compared to y_c-direction movements perpendicular to the surface of the web, yielding

$$T_{\text{flange}} = \frac{1}{2}\sigma\int_0^a (A_f v'^2 - 2A_f\xi v'\beta' + I_f\beta'^2)\,dx_1$$

The point of rotation of the flange cross section is taken to be the point centered on and at the top of the web (half-way between points 4 and 5 in Fig. 1). This selection provides continuity of the motion at the top of the web and the flange. Relative to the orientation of the bulb flat cross section, $\xi = h_f - \overline{x}$ is the vertical distance from the centroid to the point of rotation. By the parallel axis theorem, the polar moment I_f of the flange about its point of rotation is

$$I_f = I_c + A_f\left[(\overline{x}-h_f)^2 + \left(\overline{y}-\frac{1}{2}t_w\right)^2\right]$$

A lateral movement of the point of rotation $v(x_1)$ equates to $V(x_1, h_w)$. A rotation or twist about the point of rotation of the flange $\beta(x_1)$ equates to $V_3(x_1, h_w)$.

In summary, the quadratic terms of the total potential energy functional of a single stiffened plate unit at the instance of buckling can be expressed as

$$
\begin{aligned}
P_2 = {} & \frac{1}{2}D_{\mathrm{p}}\int_{-\frac{b}{2}}^{\frac{b}{2}}\int_0^a \{(W_{11}+W_{22})^2 - 2(1-\nu)[W_{11}W_{22}-W_{12}^2]\}\,\mathrm{d}x_1\,\mathrm{d}x_2 \\
& + \frac{1}{2}D_{\mathrm{w}}\int_0^{h_{\mathrm{w}}}\int_0^a \{(V_{11}+V_{33})^2 - 2(1-\nu)[V_{11}V_{33}-V_{13}^2]\}\,\mathrm{d}x_1\,\mathrm{d}x_3 \\
& + \frac{1}{2}\int_0^a (EI_{x_{\mathrm{c}}}V_{11}^2 + GJ_{\mathrm{f}}V_{13}^2)_{x_3=h_{\mathrm{w}}}\,\mathrm{d}x_1 \\
& - \frac{1}{2}\sigma\left[\int_{-\frac{b}{2}}^{\frac{b}{2}}\int_0^a t_{\mathrm{p}}W_1^2\,\mathrm{d}x_1\,\mathrm{d}x_2 + \int_0^{h_{\mathrm{w}}}\int_0^a t_{\mathrm{w}}V_1^2\,\mathrm{d}x_1\,\mathrm{d}x_3 + \int_0^a (A_{\mathrm{f}}V_1^2 + 2A_{\mathrm{f}}(\bar{x}-h_{\mathrm{f}})V_1V_{13} + I_{\mathrm{f}}V_{13}^2)_{x_3=h_{\mathrm{w}}}\,\mathrm{d}x_1\right]
\end{aligned}
\tag{8}
$$

As a consequence of continuity and assumption (iv), the boundary conditions along the plate–stiffener boundary are

$$V(x_1,0) = 0, \qquad V_3(x_1,0) = -W_2(x_1,0) \tag{9}$$

As a consequence of assumption (x), the boundary conditions on the ends of the plate and stiffener are

$$W(0,x_2) = W(a,x_2) = W_{11}(0,x_2) = W_{11}(a,x_2) = 0 \tag{10}$$

$$V(0,x_3) = V(a,x_3) = V_{11}(0,x_3) = V_{11}(a,x_3) = 0 \tag{11}$$

6. Solution to the buckling equations

The Rayleigh-Ritz method is a very effective technique that finds an approximate solution to problems formulated as an energy criterion. The method is summarized in two steps. First, assume an admissible solution containing unknown coefficients that satisfy the boundary conditions of the problem. Second, substitute the assumed solution into the functional and determine the value of the unknown coefficients that minimize the functional.

From experimental observation and by assumption (vi), the deflection of the plate panel is assumed

$$W(x_1,x_2) = \sin\frac{m\pi x_1}{a}\sin\frac{\pi x_2}{b} \tag{12}$$

The value m is the number of half-waves in the buckling mode along the longitudinal axis and is taken to be the integer that gives the lowest value for the buckling stress. The deflection of the stiffener is assumed

$$V(x_1,x_3) = -\frac{\mu h_{\mathrm{w}}}{b}\sin\frac{m\pi x_1}{a}\sin\frac{\pi x_3}{\mu h_{\mathrm{w}}}, \quad \mu \neq 0 \tag{13}$$

Here μ is an arbitrary parameter chosen to minimize the expression for the buckling stress.

Expressions (12) and (13) satisfy boundary conditions (9)–(11). Substitution of (12) and (13) into (8), and application of the stability criterion (6), yields

$$
\begin{aligned}
\sigma_{\mathrm{cr}} &\leqslant \frac{\frac{D_{\mathrm{p}}b}{2}\left(\frac{mb}{a}+\frac{a}{mb}\right)^2 + \mathrm{Term}_1 + EI_{x_{\mathrm{c}}}\left(\frac{m\pi h_{\mathrm{w}}}{a}\right)^2\left(\frac{\mu}{\pi}\sin\frac{\pi}{\mu}\right)^2 + GJ_{\mathrm{f}}\left(\cos\frac{\pi}{\mu}\right)^2}{\frac{t_{\mathrm{p}}b^3}{2\pi^2}+\frac{t_{\mathrm{w}}h_{\mathrm{w}}^3\mu^2}{2\pi^2}\left(1-\frac{\mu}{2\pi}\sin\frac{2\pi}{\mu}\right)+\mathrm{Term}_2} \\
\mathrm{Term}_1 &= \frac{D_{\mathrm{w}}h_{\mathrm{w}}}{2}\left[\left(\frac{m\mu h_{\mathrm{w}}}{a}+\frac{a}{m\mu h_{\mathrm{w}}}\right)^2\left(1-\frac{\mu}{2\pi}\sin\frac{2\pi}{\mu}\right)+4(1-\nu)\frac{\mu}{2\pi}\sin\frac{2\pi}{\mu}\right] \\
\mathrm{Term}_2 &= A_{\mathrm{f}}h_{\mathrm{w}}^2\left(\frac{\mu}{\pi}\sin\frac{\pi}{\mu}\right)^2 + 2A_{\mathrm{f}}(\bar{x}-h_{\mathrm{f}})h_{\mathrm{w}}\left(\frac{\mu}{\pi}\sin\frac{\pi}{\mu}\right)\left(\cos\frac{\pi}{\mu}\right) + I_{\mathrm{f}}\left(\cos\frac{\pi}{\mu}\right)^2
\end{aligned}
\tag{14}
$$

The lowest value of σ_{cr} in (14) is usually obtained by taking m to be one of the two integers closest to a/b. One method of determining μ is by setting equal to zero the ordinary derivative of the quotient expression (14) with respect to μ and solving for μ. We determine the parameter μ by graphical means.

Notice that in the case of a plate panel with no stiffener, only the first terms of the numerator and denominator in (14) remain and the buckling stress value is

$$\sigma_{cr} \leqslant \frac{\frac{D_p b}{2}\left(\frac{mb}{a}+\frac{a}{mb}\right)^2}{\frac{t_p b^3}{2\pi^2}} = D_p \frac{\pi^2}{t_p b^2}\left(\frac{mb}{a}+\frac{a}{mb}\right)^2 \tag{15}$$

Expression (15) agrees with the well-known solution for the buckling of a plate that has length a, width b, and is simply supported at all edges.

7. Simplified special mode buckling stress formulas

Our previous general buckling stress expression (14) involves a parameter μ, which must be determined numerically to provide the minimum value of σ_{cr}. However, we have found that the special values $\mu = 1, 2$, and $\mu \to \infty$ provide good approximations to the minimal buckling stresses, as well as insights into the buckling mode behavior.

Note further that since $m \sim a/b$, the factor $m\mu h_w/a \sim \mu h_w/b$ in Term_1 of our buckling stress formula (14) is usually negligible compared to $a/m\mu h_w \sim b/\mu h_w$. Neglecting a factor in the numerator of (14) lowers the buckling stress, whereas specializing μ in (14) raises the buckling stress, so the two approximations counteract each other.

For $\mu = 1$, the deflection mode becomes $f(x_3) = \frac{h_w}{b}\sin\frac{\pi x_3}{h_w}$ and the simplified buckling stress is

$$\sigma_{cr} \leqslant \frac{\frac{D_p b}{2}\left(\frac{mb}{a}+\frac{a}{mb}\right)^2 + \frac{D_w h_w}{2}\left(\frac{a}{mh_w}\right)^2 + GJ_f}{\frac{t_p b^3}{2\pi^2}+\frac{t_w h_w^3}{2\pi^2}+I_f} \tag{16}$$

Fig. 6a depicts the deflection of the structure corresponding to Mode 1 that is best described by a bending of the web in one half-wave and a rotation of the flange about a point at the top of the web. There is no flange bending along its length. Such a mode could occur when the flange bending stiffness is large compared to flange torsional and web bending stiffness.

For $\mu = 2$, the deflection mode becomes $f(x_3) = \frac{2h_w}{b}\sin\frac{\pi x_3}{2h_w}$ and the buckling stress is

$$\sigma_{cr} \leqslant \frac{\frac{D_p b}{2}\left(\frac{mb}{a}+\frac{a}{mb}\right)^2 + \frac{D_w h_w}{8}\left(\frac{a}{mh_w}\right)^2 + 4EI_{x_c}\left(\frac{mh_w}{a}\right)^2}{\frac{t_p b^3}{2\pi^2}+\frac{2t_w h_w^3}{\pi^2}+\frac{4A_f h_w^2}{\pi^2}} \tag{17}$$

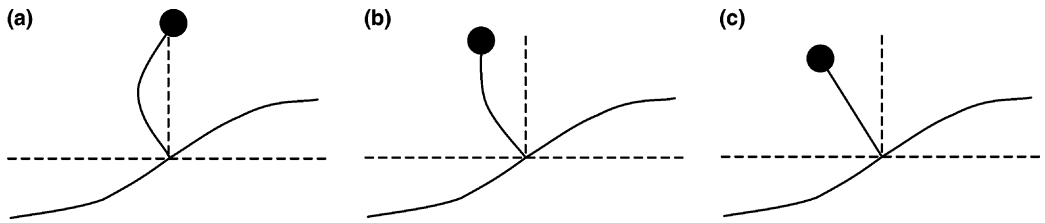

Fig. 6. (a) Mode 1 deflection, (b) Mode 2 deflection and (c) Mode 3 deflection.

Fig. 6b depicts the deflection of the structure corresponding to Mode 2. This deflection corresponds to a significant bending of the flange and web with no flange torsion. This mode could occur when the flange torsional stiffness is large compared to flange and web bending stiffness.

For $\mu \to \infty$, the deflection mode becomes $f(x_3) = \frac{\pi x_3}{b}$ and the buckling stress is

$$\sigma_{cr} \leqslant \frac{\frac{D_p b}{2}\left(\frac{mb}{a}+\frac{a}{mb}\right)^2 + \frac{Gh_w t_w^3}{3} + EI_{x_c}\left(\frac{m\pi h_w}{a}\right)^2 + GJ_f}{\frac{t_p b^3}{2\pi^2} + \frac{t_w h_w^3}{3} + A_f h_w^2 + 2A_f(\bar{x}-h_f)h_w + I_f} \tag{18}$$

Fig. 6c depicts the deflection of the structure corresponding to Mode 3. This deflection corresponds to the flange exhibiting a combination of bending and twisting while the web tends to remain straight. Such a mode could occur when the web bending stiffness is large compared to flange torsional and bending stiffness. This case is likely to occur when the flange offers little or no additional stiffness to the plate structure compared to the contribution of the web. In fact, setting the flange parameters to zero in (18), we obtain the buckling stress of a plate with a thin-webbed stiffener but no flange.

The value of μ can be interpreted to indicate the deflection behavior based on the three special deflection modes:

Mode	μ	Flange bending	Flange torsion	Web bending
1	1	No	Yes	Yes
2	2	Yes	No	Yes
3	∞	Yes	Yes	No

8. Validation of the buckling formulas using finite element models

Numerical and experimental investigations give insight about the behavior of stiffened plates and serve as a basis of comparison to theoretical predictions. Here the results of finite element analyses for several stiffened plate models using MSC Nastran 2001/Patran 2001-r3 software are compared to analytical predictions to establish a degree of confirmation.

Several simply supported rectangular plate structures serve as finite element models. Each plate structure has a plate panel of length a, width $2b$, and thickness t_p such that $t_p \ll b < a$ (Fig. 7). The stiffener divides the width of the plate in halves. Each plate panel half extends b units of length from the web to the simply

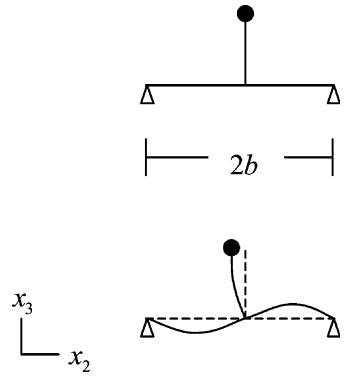

Fig. 7. Stiffened plate pre-buckling and buckling mode.

supported edge. The stiffener includes a thin web of length a, height h_w, and thickness t_w such that $t_w \ll h_w < a$. The stiffener may contain a bulb flat flange, whose cross sectional dimensions are determined by the parameters outlined earlier in this paper. Each stiffened plate structure is subjected to axial compression due to a uniform normal stress σ which increases to the buckling stress.

The derived analytical expressions in the previous section were modeled assuming a plate panel of width b. This coincides with the analysis of a single plate unit containing a single longitudinal stiffener that would be part of a larger plate structure where b units of length separate each stiffener. In this discussion, the plate structure is modeled with width $2b$, as shown in Fig. 7. The boundaries of the plate panel are now simply supported on the lateral edges, as well as the ends, leading to the additional boundary conditions

$$W(x_1,-b) = W(x_1,b) = W_{22}(x_1,-b) = W_{22}(x_1,b) = 0 \tag{19}$$

Consistency with the finite element model analysis of the $2b$ width model requires changing the limits of integration associated with the plate energy terms U_{plate} and T_{plate} from $x_2 = \pm b/2$ to $\pm b$. The fundamental problem and its mode shapes remain unchanged. Thus the only change in our previous formulas (14)–(18) is the multiplication of the first terms in the numerator and denominator by a factor of 2. The buckling stress predicted by our complete formula (14) becomes

$$\sigma_{cr} \leqslant \frac{D_p b\left(\frac{mb}{a}+\frac{a}{mb}\right)^2 + \frac{D_w h_w}{2}\left[\left(\frac{m\mu h_w}{a}+\frac{a}{m\mu h_w}\right)^2\left(1-\frac{\mu}{2\pi}\sin\frac{2\pi}{\mu}\right)+4(1-\nu)\frac{\mu}{2\pi}\sin\frac{2\pi}{\mu}\right] + EI_{x_c}\left(\frac{m\pi h_w}{a}\right)^2\left(\frac{\mu}{\pi}\sin\frac{\pi}{\mu}\right)^2 + GJ_f\left(\cos\frac{\pi}{\mu}\right)^2}{\frac{t_p b^3}{\pi^2}+\frac{t_w h_w^3\mu^2}{2\pi^2}\left(1-\frac{\mu}{2\pi}\sin\frac{2\pi}{\mu}\right)+A_f h_w^2\left(\frac{\mu}{\pi}\sin\frac{\pi}{\mu}\right)^2+2A_f(\bar{x}-h_f)h_w\left(\frac{\mu}{\pi}\sin\frac{\pi}{\mu}\right)\left(\cos\frac{\pi}{\mu}\right)+I_f\left(\cos\frac{\pi}{\mu}\right)^2} \tag{20}$$

For our finite element models with bulb flat flanges, the best simplified formula is the $\mu = 2$ case (17), which becomes

$$\sigma_{cr} \leqslant \frac{D_p b\left(\frac{mb}{a}+\frac{a}{mb}\right)^2 + \frac{D_w h_w}{8}\left(\frac{a}{mh_w}\right)^2 + 4EI_{x_c}\left(\frac{mh_w}{a}\right)^2}{\frac{t_p b^3}{\pi^2}+\frac{2t_w h_w^3}{\pi^2}+\frac{4A_f h_w^2}{\pi^2}} \tag{21}$$

For the no flange cases, we use formula (18) which becomes

$$\sigma_{cr} \leqslant \frac{D_p b\left(\frac{mb}{a}+\frac{a}{mb}\right)^2 + \frac{Gh_w t_w^3}{3}}{\frac{t_p b^3}{\pi^2}+\frac{t_w h_w^3}{3}} \tag{22}$$

A secondary aim of the finite element analysis is to estimate the effects of several variables or factors. The intention is to discern the sensitivity of the analytic expression accuracy due to the variability of web height and flange area. The web height variable is examined at two levels and the flange area at four levels. The plate panel parameters for all models remain fixed at the following values:

$a = 72$ in. $= 1829$ mm

$b = 20$ in. $= 508$ mm

$t_p = 0.3125$ in. $= 7.9375$ mm

In the Corus brochure, a 105 mm stiffener with a bulb flat flange has a web height of 84.41 mm; this is the web height used for the first set of plate models. A 120 mm stiffener with a bulb flat flange has a web height of 99.41 mm; this is the web height used for the second set of plate models. The web thickness is fixed at 6 mm. There are four flange areas examined. The first case is that for a stiffener with no flange. The remaining flange area values are derived from the following bulb flat flange parameters, where $r_1 = (1/10)t_w$ and $\alpha = \pi/6$:

Flange area level	t_w (mm)	t_{bf} (mm)	r (mm)	Area (mm^2)
1	N/A	N/A	N/A	0
2	6	17	5	335.59
3	6	20	5	401.69
4	6	25	5	523.39

Using these values, and converting the units from millimeter to inches, we obtain the parameters for the stiffened plate models given in Table 3.

Fig. 8 shows the deflection of the plate and web at the onset of buckling for model 1. The plate and web panels buckle in four half-waves along the longitudinal axis. The bulb flat flange is not visible, but its properties exist in the curve that defines the top of the web.

Fig. 9 shows the difference in the buckling behavior between models 2 and 3. In each picture, the top of the web has the beam characteristics of a bulb flat flange. The flange in the left picture has an area property of 0.6226 in.^{2}. The flange in the right picture has an area property of 0.8113 in.^{2}. These properties are not visible in the pictures, but exist in the curve that defines the top of each web. The web height in both pictures is 3.3233 in. From Table 4, the μ values for the left and right pictures are 2.57 and 2.25 respectively. This indicates there is more lateral bending of the model 2 flange at the onset of buckling, which agrees with the pictures shown.

Tables 4 and 5 give the formula predictions and finite element results. The parameter $m = 4$ in all cases.

Table 4 compares the bulb flat configurations for each model. The simplified formula values (21) are less than 4% above the finite element results. Examination of the μ values indicates that the buckling behavior of the stiffened plates tend to have significant bending of the flange and web with a degree of flange torsion.

Table 3
Summary of stiffened plate model parameters

Model #	Flange parameters	Web parameters
1	$A_f = 0.5202$ in.^{2} $t_{bf} = 0.6693$ in., $r = 0.1969$ in. $r_1 = (1/10)t_w = 0.0236$ in. $\alpha = \pi/6$ rad, $h_f = 0.8106$ in.	$h_w = 3.3233$ in. $t_w = 0.2362$ in.
2	$A_f = 0.6226$ in.^{2} $t_{bf} = 0.7874$ in., $r = 0.1969$ in. $r_1 = (1/10)t_w = 0.0236$ in. $\alpha = \pi/6$ rad, $h_f = 0.8788$ in.	$h_w = 3.3233$ in. $t_w = 0.2362$ in.
3	$A_f = 0.8113$ in.^{2} $t_{bf} = 0.9843$ in., $r = 0.1969$ in. $r_1 = (1/10)t_w = 0.0236$ in. $\alpha = \pi/6$ rad, $h_f = 0.9924$ in.	$h_w = 3.3233$ in. $t_w = 0.2362$ in.
4	Same as model 1	$h_w = 3.9138$ in. $t_w = 0.2362$ in.
5	Same as model 2	$h_w = 3.9138$ in. $t_w = 0.2362$ in.
6	Same as model 3	$h_w = 3.9138$ in. $t_w = 0.2362$ in.

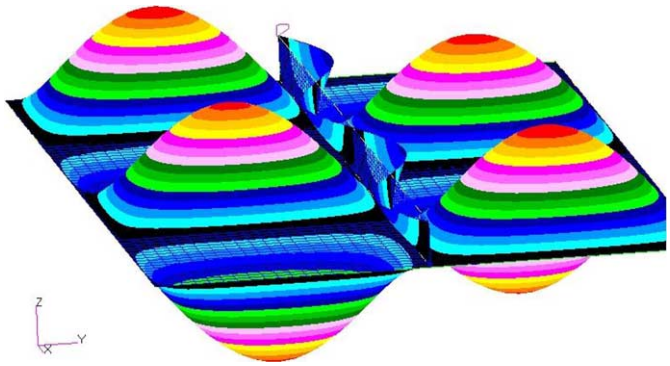

Fig. 8. MSC Patran picture for stiffened plate model 1.

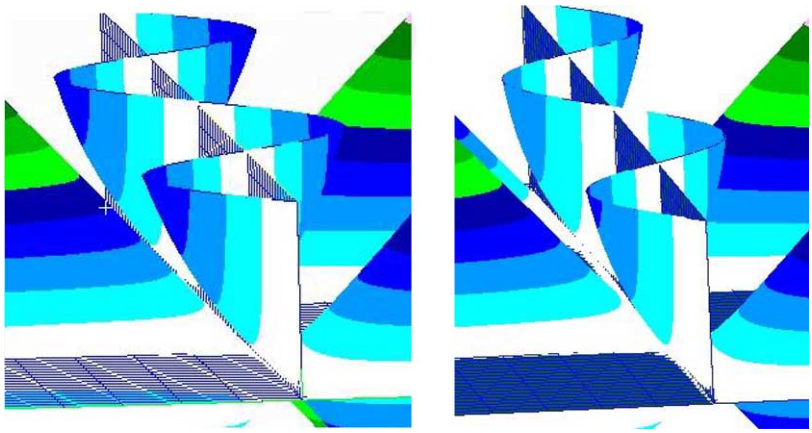

Fig. 9. MSC Patran pictures showing the buckling behavior of the webs with bulb flat flanges for models 2 (left) and 3 (right).

Table 4
Bulb flat FE results

Model #	FE results (psi)	Formula (20) (psi)	μ	Formula (21) (psi)	$100 * ((21)-FE)/FE$ (%)
1	27,672	28,397	2.86	28,554	3.19
2	27,877	28,824	2.57	28,763	3.18
3	28,203	29,642	2.25	29,301	3.89
4	27,663	28,425	2.68	28,264	2.17
5	27,881	28,908	2.40	28,552	2.41
6	28,217	29,852	2.11	29,292	3.81

Table 5
No flange FE results

Model #	FE results (psi)	Formula (22) (psi)	$100 * ((22) - FE)/FE$ (%)
1–3	26,928	27,129	0.75
4–6	26,892	27,052	0.59

This type of buckling behavior can be seen in the Patran pictures on the previous page. As the flange areas increase between models 1, 2, and 3, and also between models 4, 5, and 6, the μ values tend to approach the value 2, indicating perhaps an increasing torsional rigidity effect. The buckling stresses tend to increase as the flange area increases, as expected. Overall, the results indicate that at the onset of buckling, the bulb flat stiffened plate structures deflect with a combination of flange bending and torsion along with web bending.

Table 5 compares the results for the stiffened plates without flanges. The formula values nearly agree with the finite element results.

From finite element results, the buckling stress of a plate with a bulb flat stiffener is 3–4% less than that of a plate with a T flange stiffener of the same cross sectional area. See Wilmer (2003) for more details on the buckling of plates with stiffener flanges of T and other cross sections.

9. Summary

The following summarizes our major findings and conclusions, followed by explanatory comments.

- Determined cross sectional boundary equations for the bulb flat flange cross section.

In order to conduct an accurate analysis of the bulb flat cross section, it is necessary to determine equations that define or at least approximate the boundary that is a closed bounded plane region. The equation that defines the boundary of a simple geometric cross section like a circle or ellipse is well known. The boundary equation for uncommon and asymmetric cross sections is often very difficult to define. As a result of this study, functions exist that define the boundary of the bulb flat flange cross section.

- Derived planar property value expressions.

Determining the critical buckling stress of a stiffened plate structure requires knowledge of several planar property values of the plate's cross section. Based on the boundary equations and the application of multivariable calculus, a double integral provides expressions for calculating the various planar properties of the bulb flat flange cross section. Though the integral expressions are complicated, they could be simplified by assigning fixed values to certain variables.

- Determined an approximate torsional constant expression that is more accurate than idealizing.

The Saint-Venant torsional constant is one of the key property values involved in the analysis of stiffened plate structures. Due to the uncommon shape and asymmetrical property of the bulb flat cross section, determining the exact expression for the Saint-Venant torsional constant is difficult and does not exist in published literature. As a result of this study, an empirical expression exists for the Saint-Venant torsional constant of a specified class of bulb flat cross sections. The empirical expression is a one-term function involving the flange cross sectional area and polar moment of inertia.

- Demonstrated that the torsional property of the bulb flat stiffener is now understood better than previously. The torque-carrying capacity of a bulb flat stiffener is greater than that of an area-equivalent angle stiffener.

In previous investigations the torsional nature of the bulb flat stiffener was idealized as an angle flange stiffener. That is, the bulb flat flange cross section was treated like a rectangular cross section in regards to the torsional and warping properties. Such treatment imputed error in the calculation of the bulb flat

stiffener's torsional rigidity resulting in conservative estimates. Finite element analysis indicates that the torque-carrying capacity of a bulb flat stiffener (possessing no structural flaws) is greater than that of an area-equivalent angle stiffener.

- Derived general expressions to predict the buckling stress due to the stiffener tripping of a simply supported rectangular stiffened plate subjected to axial compression. For stiffeners with a bulb flat flange, the values predicted with a simple formula are less than 4% higher than the finite element results.

Understanding the elastic stability of stiffened plate structures is important to the analyst, designer, and educator involved in the analysis and design of structures. Use of the energy method provides a technique to derive a general expression for the buckling stress due to the stiffener tripping of a simply supported rectangular stiffened plate subjected to axial compression. As a result of this study, a useful analytic expression exists that allows the user to predict the critical buckling stress and the buckling behavior of a stiffened plate at the onset of stiffener tripping. The onset of stiffener tripping negates the stiffener's support to the plate panel and leads to eventual collapse of the structure. The general expressions involve a parameter μ, determined graphically, that can be interpreted to indicate the deflection behavior. Simplified buckling stress formulas corresponding to Mode 2 ($\mu = 2$) give even better predictions for the modeled structures.

10. Comparison with experimental results

Careful experiments on large-scale multi-bay grillages have been performed by Kihl (2003). A grillage with bulb flat stiffeners failed in the tripping manner postulated in this paper. The minimum critical elastic buckling stress σ_{cr} was obtained from Eq. (17) for Mode 2. The ultimate failure stress σ_{crinel} was then determined from the following equation:

$$\sigma_{crinel} = \sigma_y \left[1 - p_r(1 - p_r)\left(\frac{\sigma_y}{\sigma_{cr}} \right) \right] \quad \text{for } p_r\sigma_y < \sigma_{cr} < \sigma_y \tag{23}$$

Here $p_r = 0.5$ is the ratio of the structural proportional limit to the yield strength σ_y. Using measured values for geometrical and material parameters, Kihl (2003) calculated a force which is only 3.7% less than his measured ultimate failure load of 1.34 million pounds.

Acknowledgements

The authors were supported by the Naval Surface Warfare Center and the Naval Postgraduate School research programs. Dr. Dave Kihl of NSWC proposed the title problem and offered many valuable suggestions. Dr. John Adamchak of NSWC also provided significant insights.

References

Bleich, F., 1952. Buckling Strength of Metal Structures. McGraw-Hill Book Co.

Byklum, E., Amdahl, J., 2002. A simplified method for elastic large deflection analysis of plates and stiffened panels due to local buckling. Thin-Walled Structures 40, 925–953.

Chajes, Alexander, 1974. Principles of Structural Stability Theory. Prentice-Hall.

Chou, S.K.G., 1997. Design of longitudinally stiffened plating in compression with particular reference to torsional buckling. Ph.D. Thesis, Civil Engineering Department, Imperial College, London.

Chou, S.K.G., Chapman, J.C., 2000. Local critical buckling of bulb flat stiffened plating. The Structural Engineer 78 (8), 24–29.
Chou, S.K.G., Chapman, J.C., Davidson, P.C., 2000. Design of bulb flat stiffened plating. The Structural Engineer 78 (18), 24–32.
Corus Group, 2002. Bulb flats. Available from <http://www.corus-specialprofiles.com/pdf/Bulbflat.pdf>.
Danielson, D.A., 1974. Theory of Shell Stability. Thin-Shell Structures. Prentice-Hall. pp. 45–58.
Danielson, D.A., 1995. Analytical tripping loads for stiffened plates. International Journal of Solids and Structures 32 (8/9), 1319–1328.
Danielson, D.A., Kihl, D.P., 1996. Buckling of ship grillages. Naval Postgraduate School Technical Report NPS-MA-96-002.
Danielson, D.A., Kihl, D.P., 1997. Buckling of ship grillages—Part II. Naval Postgraduate School Technical Report NPS-MA-97-005.
Danielson, D.A., Kihl, D.P., Hodges, D.H., 1990. Tripping of thin-walled plating stiffeners in axial compression. Thin-Walled Structures 10, 121–142.
Danielson, D.A., Cricelli, A.S., Frenzen, C.L., Vasudevan, N., 1993. Buckling of stiffened plates under axial compression and lateral pressure. International Journal of Solids and Structures 30 (4), 545–551.
Danielson, D.A., Steele, C.R., Fakhroo, F., Cricelli, A.S., 1994. Stresses in ship plating. Naval Postgraduate School Technical Report NPS-94-008.
Donaldson, B.K., 1993. Analysis of Aircraft Structures: An Introduction. McGraw-Hill.
Kihl, D.P., 2003. Test results of grillages with asymmetric stiffeners. Naval Surface Warfare Center Carderock Division Technical Report NSWCCD-65-TR-2003/45.
Timoshenko, S.P., Gere, J.M., 1961. Theory of Elastic Stability, second ed. McGraw-Hill.
Timoshenko, S.P., Goodier, J.N., 1970. Theory of Elasticity, third ed. McGraw-Hill.
Wilmer, A., 2003. Analytic expression of the buckling loads for stiffened plates with bulb flat flanges. Ph.D. Thesis, Department of Applied Mathematics, Naval Postgraduate School, Monterey, CA.